Cell, Vol. 86, 799–810, September 6, 1996, Copyright ©1996 by Cell Press

Inactivation of the HR6B Ubiquitin-Conjugating DNA Repair Enzyme in Mice Causes Male Sterility Associated with Chromatin Modification

H. P. Roest,* J. van Klaveren,* J. de Wit,* C. G. van Gurp,* M. H. M. Koken,*§ M. Vermey,‡ J. H. van Roijen,† J. W. Hoogerbrugge,† J. T. M. Vreeburg,† W. M. Baarends,† D. Bootsma,* J. A. Grootegoed,† and J. H. J. Hoeijmakers*

*MGC–Department of Cell Biology and Genetics
†Department of Endocrinology and Reproduction
‡Department of Pathology
Faculty of Medicine and Health Sciences
Erasmus University Rotterdam
3000 DR Rotterdam
The Netherlands

Summary

The ubiquitin-conjugating yeast enzyme RAD6 and its human homologs hHR6A and hHR6B are implicated in postreplication repair and damage-induced mutagenesis. The yeast protein is also required for sporulation and may modulate chromatin structure via histone ubiquitination. We report the phenotype of the first animal mutant in the ubiquitin pathway: inactivation of the *hHR6B*-homologous gene in mice causes male infertility. Derailment of spermatogenesis becomes overt during the postmeiotic condensation of chromatin in spermatids. These findings provide a parallel between yeast sporulation and mammalian spermatogenesis and strongly implicate hHR6-dependent ubiquitination in chromatin remodeling. Since heterozygous male mice and even knockout female mice are completely normal and fertile and thus able to transmit the defect, similar hHR6B mutations may cause male infertility in man.

Introduction

The ubiquitin system plays a key role in numerous cellular processes, including metabolic homeostasis, stress response, organelle biosynthesis, cell cycle regulation, DNA repair, apoptosis, antigen processing, and gene expression (for recent reviews, see Ciechanover, 1994; Hochstrasser, 1995). This selective, nonlysosomal proteolytic pathway mediated by the 26S protease complex determines the half-life of crucial proteins such as p53, cyclins, transcription factors, and cytosolic polypeptides (Chau et al., 1989; Ciechanover et al., 1991; Glotzer et al., 1991; Kornitzer et al., 1994; Seufert et al., 1995). Furthermore, this pathway is implicated in stabilization, refolding, and translocation of a diverse range of proteins. The ubiquitin pathway involves a three- or four-step ubiquitin thioester cascade. The highly conserved 76 amino acid ubiquitin molecule is first activated by the ubiquitin-activating enzyme (E1) through formation of a high energy thioester linkage of its C-terminal glycine with a cysteine residue in the E1 protein itself. Subsequently, the ubiquitin moiety is transferred to a cysteine of one of the ubiquitin-conjugating (UBC or E2) enzymes, which in turn attaches the ubiquitin part onto a target protein with or without the assistance of a ubiquitin-protein ligase (E3). The latter step may involve a third thioester linkage with the E3 enzyme (Scheffner et al., 1995) and results in the formation of an isopeptide bond of the activated C-terminal glycine of ubiquitin with the N-terminus or the ϵ-NH2 group of an internal lysine residue of the substrate polypeptide. Polyubiquitination is thought to mark proteins for degradation, whereas mono-ubiquitination may serve other functions (Chau et al., 1989).

A key role in this pathway is exerted by a growing family of UBC enzymes, which in yeast already comprises 12 members (Hochstrasser, 1995). An extreme example of the pleiotropic involvement of this class of proteins in cellular processes is presented by the yeast S.cerevisiae *RAD6* gene product. Strains mutated in *RAD6* display defects in postreplication daughter strand gap repair, causing pronounced sensitivity to all kinds of DNA damaging agents, increased spontaneous mutation frequency and concomitant loss of damage-induced mutagenesis. In addition, *rad6* null alleles exhibit cell cycle perturbance, temperature-sensitive growth, inability to sporulate, and increased retrotransposition (see Lawrence, 1994). The crucial finding concerning the function of the protein was made by Jentsch et al. (1987), who identified RAD6 as the first ubiquitin-conjugating enzyme, able to mono- and polyubiquitinate histones 2A and 2B in vitro. The protein has been demonstrated to mediate N-end rule protein degradation (Dohmen et al., 1991), and its highly conserved N-terminus is implicated in interaction with the UBR1 protein (Madura et al., 1993). Its in vitro ability to ubiquitinate histones has led to the suggestion that RAD6 mediates its functions by modulating chromatin structure as an essential part of the DNA transactions (repair, replication) in which it is implicated. However, direct demonstration of the role of the protein in chromatin dynamics is still lacking. In normal mammalian cells, a substantial fraction of histone H2A and, to a lesser extent, H2B is present in a ubiquitinated form (Goldknopf and Busch, 1980; Thorne et al., 1987). Although histones are frequently utilized as substrates for ubiquitin conjugation, the function of ubiquitination of histones in vivo is largely unexplored, and it is unknown whether and to what extent RAD6 is involved in this posttranslational modification.

Previously, we cloned *RAD6* homologs of several higher eukaryotes including two closely related human homologs, designated *hHR6A* and *hHR6B* (for *h*uman *H*omologs of *RAD6*) (Koken et al., 1991b). The encoded human proteins are both structurally and functionally highly conserved: they share ~70% sequence identity with S. cerevisiae RAD6 and are able to ubiquitinate histones in vitro, and both human gene products can substitute for the mutagenesis and UV resistance function of the yeast protein but not for its role in sporulation.

§Present address: CNRS UPR90-51 Pathologie Cellulaire: Aspects Moléculaire et Viraux, Hôpital St. Louis, 1 Avenue Claude Vellefaux, 75475 Paris Cedex 10, France.

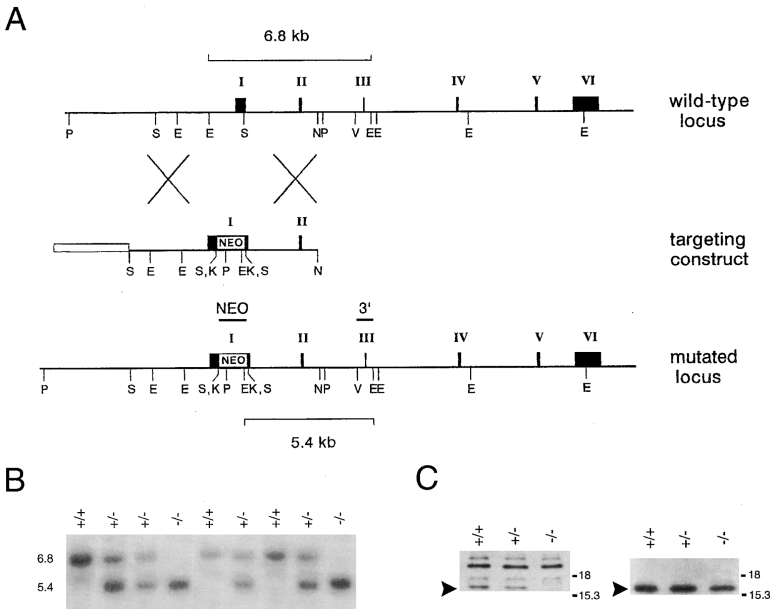

Figure 1. Targeted Disruption of the *mHR6B* Gene by Homologous Recombination

(A) Genomic organization and disruption strategy for *mHR6B* showing the gene, the targeting construct, and the targeted *mHR6B* allele. The *neo* cassette is inserted in the SalI site of exon 1, introducing a diagnostic EcoRI site. Note that insertion of the dominant marker disrupts the gene immediately behind the ATG translation initiation codon. Shown are the relevant restriction sites (E, EcoRI; S, SalI; N, NsiI; K, KpnI; V, EcoRV; P, SphI). The position of the 3′ probe and the neo probe for Southern blot analysis are indicated above the mutated locus. Lines on top and bottom indicate the estimated length of the fragments detected in Southern blot analysis of EcoRI digested DNA. Roman numerals mark the exons.

(B) Southern analysis of EcoRI digested DNA from nine littermates after hybridization with the 3′ probe. The positions of the wild-type allele (6.8 kb) and the targeted allele (5.4 kb) are indicated.

(C) Western blot analysis of testes extract of wild-type (+/+), heterozygous (+/−) and homozygous mutant (−/−) animals. In the left panel mHR6B protein was detected using the antiserum raised against the C-terminus of mHR6B/hHR6B (α-AB1). In the right panel the reaction with the α-RAD6 antiserum is presented. On the left of both panels the position of mHR6B is indicated (arrowheads); on the right side, the positions of the relevant molecular weight markers are shown.

This latter function requires in S. cerevisiae an acidic C-terminal extension. In S. pombe however, like in the Drosophila and mammalian homologs, the acidic tail is absent and not needed for sporulation (Reynolds et al., 1990; Schneider et al., 1990; Koken et al., 1991a, 1991b). The subcellular localization of HR6 in the euchromatic regions of the nucleus (Koken et al., 1996) suggests that its function is related to active chromatin conformation. Both mammalian genes are expressed in all organs and tissues and are not subject to mitotic cell cycle regulation. Furthermore, expression of both genes is elevated in mouse spermatids (postmeiotic spermatogenic cells), coinciding with the developmental steps at which a complex series of chromatin modification events takes place (Koken et al., 1996). These events involve replacement of somatic and testis-specific histones by transition proteins TP1 and TP2, and subsequently by protamines P1 and P2 (Balhorn, 1989; Kistler, 1989; Meistrich, 1989). In rat spermatids, occurrence of highly acetylated histone H4 is found to be associated with histone displacement (Meistrich et al., 1992). Ubiquitination of histones and other nuclear proteins might also be involved in this process, because ubiquitination of histones has been observed during chicken and trout spermatogenesis (Agell et al., 1983; Nickel et al., 1987; Agell and Mezquita, 1988; Oliva and Dixon, 1991).

Studies on the biological and molecular function of HR6 and other enzymes implicated in the ubiquitin pathway in higher organisms are hampered by lack of mutants. The central role of *RAD6* in multiple processes makes it an interesting target for generating a knockout mouse mutant. Here we demonstrate that mice deficient for the murine version of HR6B (mHR6B) are viable and phenotypically normal, presumably due to functional redundancy with mHR6A. The mHR6B-deficient male mice, however, are infertile, whereas mHR6B-deficient females show normal fertility. The defect in spermatogenesis is consistent with impairment of the complex postmeiotic chromatin remodeling process and provides evidence for involvement of the ubiquitin pathway in chromatin dynamics. Moreover, our findings may have clinical implications for understanding male infertility in man.

Results

Main Features of the Mouse *HR6B* Gene and cDNA

To permit the design of targeting constructs, mouse cDNAs and the corresponding gene were isolated using cross-hybridization to a human HR6B (*hHR6B*) probe. To facilitate homologous recombination with high efficiency, the mouse homolog of *RAD6* (*mHR6B*) was cloned from a λ phage library of genomic mouse strain 129/Sv DNA, isogenic to the embryonal stem cell line used for gene targeting. The high conservation of the gene is apparent from the finding that its predicted amino acid sequence is completely conserved between mouse and man. A notable feature is the 100% conservation of a sequence of at least 309 base pairs in the 3′UTR of the *mHR6B* mRNA between all mammals investigated (man, mouse, rat, and rabbit). This stretch corresponds with nucleotides 575 to 884 of the published human cDNA sequence (Koken et al., 1991b). To our knowledge, this represents the longest nucleotide stretch strictly preserved over such an evolutionary distance. The function of this exceptionally stable, noncoding nucleotide sequence element is unknown.

Figure 1A presents the architecture of the murine *mHR6B* gene. The gene spans a region of ~15 kb and is comprised of six exons. Interestingly, the location of two introns is exactly preserved in Drosophila and even S. pombe (Reynolds et al., 1990; Koken et al., 1991a),

presumably reflecting a high importance for the gene. The gene was mapped on mouse chromosome 13 in a region syntenic with human chromosome 5, and evidence was obtained for a pseudogene on mouse chromosome 11 (Roller et al., 1995).

Inactivation of the *mHR6B* Gene and Generation of Mouse Mutants

In designing a knockout targeting construct, we envisioned the possibility that any truncated mHR6B protein may exert unpredictable effects. Particularly, the highly conserved N-terminus, encoding a site for protein–protein interaction, could interfere with other processes resulting in semidominant consequences. Therefore, we chose to inactivate the *mHR6B* gene immediately after the translational start codon by insertion of the dominant-selectable neomycin or hygromycin marker, ruling out the synthesis of any part of the protein. The targeting construct depicted in Figure 1A contains 3.5 kb and 2.8 kb of homology at the 5′ and 3′ side flanking the dominant-selectable marker, respectively. Two versions, each with a different selectable marker, were constructed to permit inactivation of both autosomally located alleles in ES cells.

Transfection of the *neo* cassette–containing targeting construct (Figure 1A) by electroporation and selection for stable uptake of the dominant selectable marker gene yielded a frequency of 16% targeted transformants (27 homologous recombinants/166 total transformants—no selection was applied against random integration). Homologous recombinants were checked for accurate integration of the construct by Southern blot analysis using external and internal probes and were found to be correct (data not shown).

The multiple engagements of RAD6 on the one hand and the presence of a 95% identical mHR6A protein on the other, make it difficult to predict a phenotype for a mHR6B-deficient mouse. To find out whether a homozygous *mHR6B* inactivation is viable, at least at the cellular level, the second allele was targeted using the *hygro* cassette-containing construct. The frequency of targeting directed to the wild-type allele was 8% (11/143), indicating that there was no selection against *mHR6B* inactivation and that inactivation of both *mHR6B* alleles is not lethal. Therefore, we performed injection of ES cells of two independent, neomycin-resistant clones (80 and 134) into blastocysts of C57BL/6 mice, resulting in the generation of chimaeras. Male chimaeras from both independent clones were bred and both gave germline transmission. Southern blot analysis on DNA isolated from tail biopsies was used to determine the genotype of the offspring. Hybridization with the 3′ external probe visualized a 6.8 kb EcoRI fragment in the case of a normal allele and a 5.4 kb fragment for a targeted allele (Figure 1B). Heterozygotes were interbred and yielded homozygous *mHR6B* mutants with the expected Mendelian frequency. The results of a representative litter are shown in Figure 1B.

We verified that the targeting of *mHR6B* indeed resulted in a null mutation at the RNA and protein levels. Northern blot analysis confirmed the absence of significant amounts of *mHR6B* transcripts (data not shown), indicating that the presence of the dominant marker interfered with proper transcription and/or processing of the altered mRNA. The mHR6A and mHR6B proteins, like hHR6A and hHR6B, are 95% identical and migrate at the same molecular weight in SDS–polyacrylamide gel electrophoresis. To distinguish between these highly homologous polypeptides, we took advantage of the fact that within the 14 C-terminal amino acids, the A and B products differ at 2 positions. A peptide identical to the 14 C-terminal amino acids of HR6B was synthesized and utilized to raise a polyclonal antiserum that specifically recognizes this protein. Since in testis both proteins are expressed in high quantities, total testis extracts were analyzed. Figure 1C (left panel) shows that no mHR6B protein is detected in $mHR6B^{-/-}$ mice, whereas the protein is present in $mHR6B^{+/-}$ and $mHR6B^{+/+}$ littermates. The decrease in intensity in the testis extract of the heterozygous animal suggests that these animals contain roughly half the amount of mHR6B protein as compared with the normal animals. This argues against upregulation of the untargeted allele to compensate for the loss of expression of the targeted copy. An antiserum against yeast RAD6, recognizing both HR6A and HR6B (Koken et al., 1996), shows a positive reaction in the $mHR6B^{-/-}$ sample, indicating that the *mHR6A* gene is expressed (Figure 1C, right panel). These results verify the null status of the *mHR6B* mutation and also show that mHR6A protein is still present.

Phenotypic Characteristics of $mHR6B^{-/-}$ Mice and Cells

The $mHR6B^{-/-}$ mice proved normally viable with a life span exceeding 14 months. Except for the feature discussed below, no apparent phenotypical or pathological abnormalities were found. Furthermore, no differences were noted between the main phenotypic characteristics of the $mHR6B^{-/-}$ mice derived from the independently targeted ES recombinants and between mice from crossings between different strains (129xFVBJ, 129x C57BL6). This rules out the possibility that by accident other genetic alterations had occurred that might influence the phenotype or that the genetic background is of major importance. Since RAD6 in yeast accounts for much of the cellular resistance against a wide spectrum of genotoxic agents, we investigated UV and γ-ray sensitivity in mouse cells. To test UV sensitivity, mouse embryonic fibroblast cell lines were established from *mHR6B* +/+, +/−, and −/− mice and tested for their cellular survival, as measured by [^{3}H]thymidine incorporation, after irradiation with different doses of UV. For γ-ray sensitivity, the double-targeted ES cell line was irradiated and cloning efficiency was compared with irradiated, nontargeted ES cells. No differences between mHR6B-deficient and -proficient cells were observed for these DNA damaging agents (data not shown). Thus no overt defect in DNA repair was detected. This is possibly caused by a redundant effect of a functional *mHR6A* gene.

Spermatogenesis in mHR6B-Deficient Mice

In breeding experiments, it soon became apparent that the $mHR6B^{-/-}$ male mice were consistently infertile.

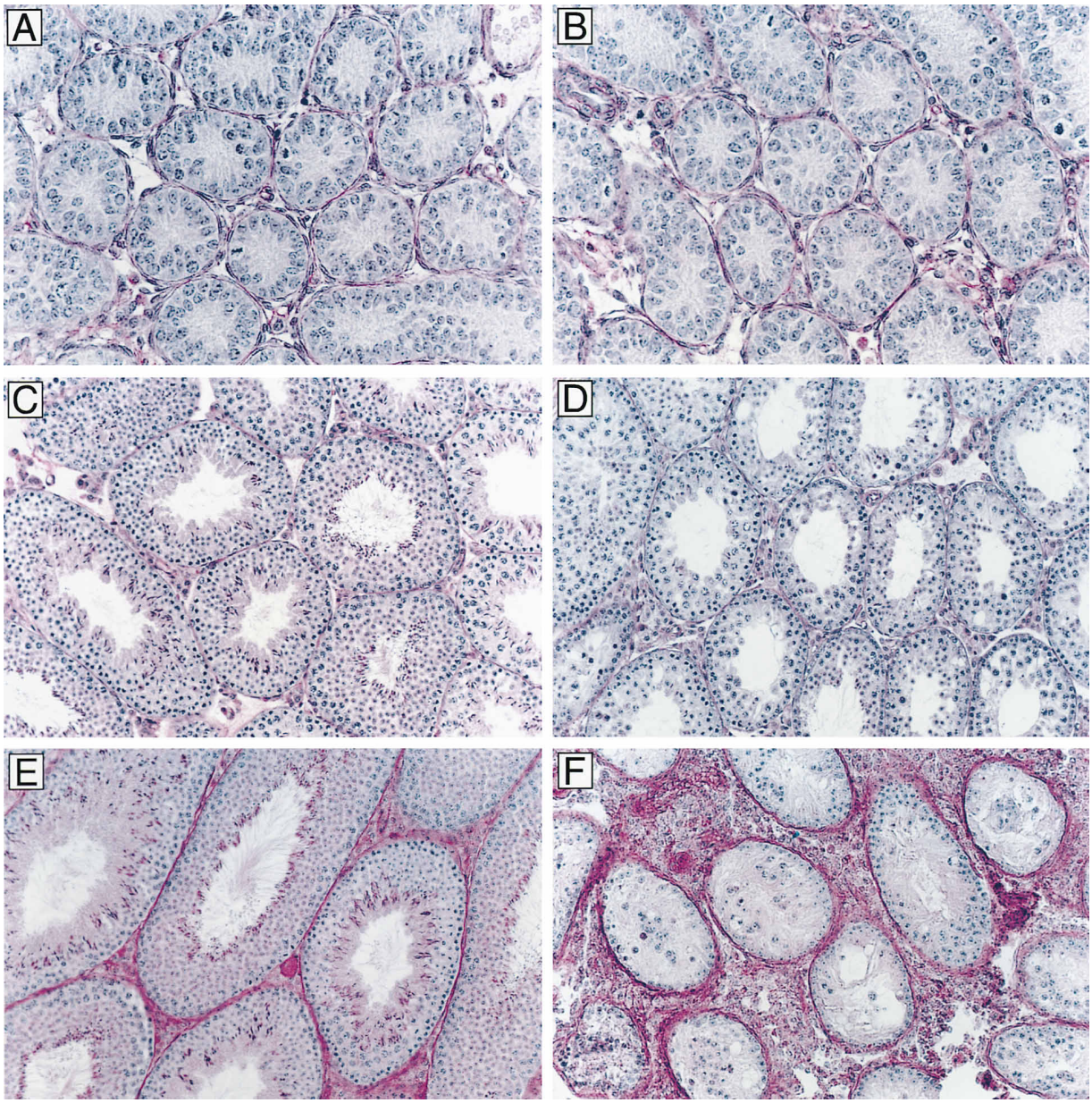

Figure 2. Testicular Histology of Normal and *mHR6B* Knockout Mice

The histological sections were prepared as described in the Experimental Procedures and stained with periodic acid Schiff (PAS). The panels to the left (A, C, and E) show the testicular histology of normal mice; the panels to the right (B, D, and F), that of knockout animals. (A) and (B): 8-day-old mice (×400); (C) and (D): 40-day-old mice (×200); (E) and (F): 9-month-old mice (×200).

Copulatory behavior was judged to be normal, and copulation plugs were found; however, none of the tested males induced pregnancy in fertile females (out of at least 27 matings with 11 knockout males no pregnancies were recorded). Histological evaluation of the testes and epididymides of adult *mHR6B*$^{-/-}$ males showed a strong derailment of spermatogenesis (>10 males investigated). However, considerable variation in the severity of the deficiencies in different adult mice was observed, involving early as well as later steps of spermatogenesis, precluding identification of the exact step at which spermatogenesis is affected. Therefore, the onset of spermatogenesis was closely followed in these mice.

In immature *mHR6B*$^{-/-}$ mice, an intact tubular structure with normal development of Sertoli cells was observed (Figures 2A and 2B). Subsequently, initiation of spermatogenesis showed no overt abnormalities, with proper development of spermatogonia, and timely onset and progression of the meiotic prophase and divisions. It is unlikely that mHR6B is indispensable for meiosis, also because the *mHR6B*$^{-/-}$ females showed normal fertility (data not shown). Clear signs of spermatogenic failure were observed when the first waves of spermatogenic cells reached the more advanced steps of spermiogenesis, in 4- to 5-week-old *mHR6B*$^{-/-}$ mice (mice analyzed at 8 days, 2.5, 3.5, 4.5, and 5.5 weeks). In

Table 1. Body and Organ Weights, and Epididymal Sperm Count in Normal and *mHR6B* Knockout Mice

	Intact[a] (Mean ± SD)	Knockout[b] 1	2	3
Body weight (g)	44 ± 6	40	49	63
Testis (mg)	99 ± 17	55	26	48
Epididymis (mg)	42 ± 5	38	29	39
Seminal vesicles (mg)	109 ± 16	86	79	109
Sperm count ($\times 10^6$)	15.5 ± 2.7	0.9	<0.1	0.9

[a] Control group consisted of five 8-month-old mice (two +/+ and three +/−).
[b] Individual data of three 8-month-old −/− mice (numbers 1, 2, and 3).

general, the spermatogenic epithelium started to show a number of irregularities, including the formation of vacuoles within the epithelium and shedding of immature germ cells, in particular round and more advanced spermatids. Figures 2C and 2D show histological sections of testes from control and knockout mice isolated at the age of 40 days. From this point on, heterogeneity in testicular histology and variation in regression of spermatogenesis was observed between individual mice. Occasionally (in 10%–20% of mHR6B$^{-/-}$ males) a nearly total absence of all germ cell types was found (Figure 2F), but in most knockout males we registered ongoing spermatogenesis with only low numbers of predominantly abnormal spermatozoa (see below).

A marked but variable reduction in testis weight (Table 1) illustrated the pronounced overall regression of spermatogenesis, although interindividual heterogeneity was apparent. In *mHR6B*$^{-/-}$ mice numbers 1 and 3 (Table 1), the epididymis weights were not significantly decreased, despite the fact that the epididymal sperm counts were <10% of the numbers found in *mHR6B* +/+ and +/− mice. This is probably explained by the abundant presence of immature germ cells in the epididymal lumen (compare Figures 5C and 5D). Epididymis weight of mutant mouse number 2 was lower, owing to the complete absence of germ cells. Mutant mice numbers 1 and 3 still contained many immature germ cells in the epididymal lumen.

Seminal vesicle weight is an excellent marker of long-term testosterone action, and the data in Table 1 therefore indicate that the plasma testosterone concentration in the *mHR6B* knockout mice was maintained within the normal range. Furthermore, the plasma follicle-stimulating hormone (FSH) concentration was not different between mHR6B-deficient mice (37, 38, and 51 ng/ml in three mice) and intact mice (40 ± 6 ng/ml in five mice).

To study the remaining spermatozoa of *mHR6B*$^{-/-}$ mice in more detail, morphology and motility were examined using Nomarski optics of unfixed material and phase contrast microscopy, respectively. In knockout mice >90% of the spermatozoa were clearly morphologically abnormal. At least 70% of these spermatozoa had an aberrant head morphology, in most cases combined with middle piece deformation (see Figure 3). Moreover, the residual spermatozoa appeared almost immotile: a few spermatozoa (~5%) displayed a sluggish progressive or nonprogressive motility. These findings confirmed that the *mHR6B* gene knockout does not cause

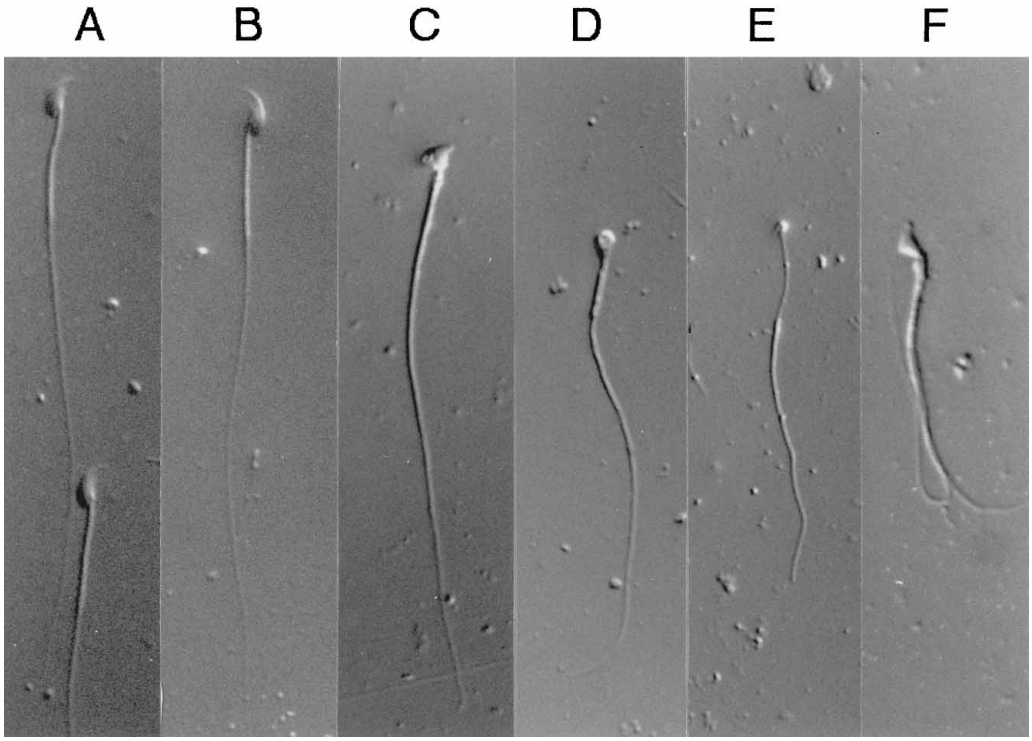

Figure 3. Normal and Abnormal Morphology of Spermatozoa from *mHR6B* Knockout Mice

The spermatozoa were collected from the cauda epididymis, and photographed without fixation using Normarski optics (×352). (A), normal; (B)–(F), abnormal.

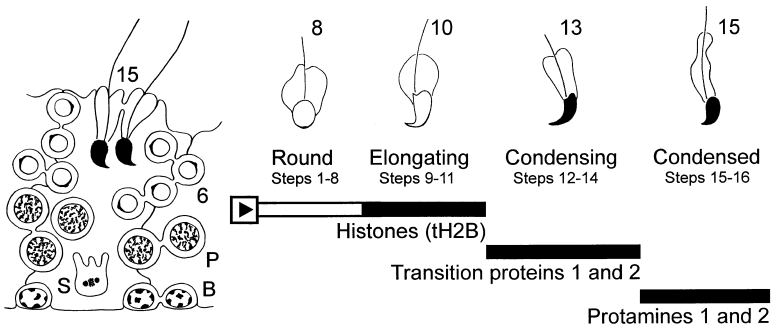

Figure 4. Schematic Presentation of the Histone-to-Protamine Replacement in Mouse Spermatids

The diagram to the left is a schematic representation of a part of a cross-section of a tubule at stage VI of the spermatogenic cycle (Russell et al., 1990) showing the interrelationship between a Sertoli cell (S), spermatogonia type B (B), pachytene spermatocytes (P), round spermatids step 6 (6), and condensing spermatids step 15 (15). The right part of the figure shows selected steps of spermatid development (steps 8, 10, 13, and 15 of spermiogenesis). The bars represent (from left to right) the following: testis-specific histone 2B (tH2B) is present in round spermatids (and in spermatocytes), but the immunoexpression of this protein is increased in elongating spermatids steps 9–11 (Unni et al., 1995); nuclear deposition of transition proteins 1 and 2 (TP1 and TP2) occurs in condensing spermatids steps 12–14 (Alfonso and Kistler, 1993), followed by replacement of the TPs by the protamines (P1 and P2).

a complete and uniform block of spermatogenesis at a given point in adult animals.

The low number of cells at the critical step where the first abnormalities were seen precluded biochemical analysis of these cells in the *mHR6B*$^{-/-}$ mice. However, the impairment of spermatogenesis in these mice was defined more precisely, using immunohistochemistry. As an introduction to these studies, a brief description of chromatin rearrangement during spermatogenesis, in particular during the postmeiotic development of spermatids (spermiogenesis), is presented (see also Figure 4).

Spermatogonia, proliferating through mitotic divisions, contain somatic histones. With the progression of spermatogenesis, a number of testis-specific histones (tH2B) are synthesized, mainly in primary spermatocytes, during the prophase of the meiotic divisions. The round and elongating spermatids contain a mixture of somatic and testis-specific histones (Brock et al., 1980; Meistrich et al., 1985). Following the elongation phase (steps 9–11 of spermiogenesis in the mouse), the elongated spermatids start with the process of nuclear condensation (steps 12–14), involving the synthesis of transition proteins 1 and 2 (TP1 and TP2) and protamines 1 and 2 (P1 and P2). The transition proteins appear in the nucleus at step 12 and are lost at step 14 when further condensation of the nucleus takes place, concurrent with the nuclear deposition of the protamines (Kistler, 1989; Meistrich, 1989; Alfonso and Kistler, 1993).

Testis-specific histone H2B (tH2B) is synthesized and deposited onto the chromatin, beginning in early primary spermatocytes (Brock et al., 1980; Meistrich et al., 1985). It represents a good marker for the elongation phase, showing intense immunostaining, due to increased accessibility of the epitope in spermatids (Unni et al., 1995). Figures 5A and 5B show that the tH2B-immunopositive spermatids that remain present in the testis of *mHR6B*$^{-/-}$ mice, display an irregular orientation and distribution, in contrast to the well-organized structure of the spermatogenic epithelium in control mice (Figures 5A and 5B). Interestingly, tH2B-immunopositive cells were also detected in the lumen of the epididymis of *mHR6B*$^{-/-}$ mice (Figure 5D). These cells were virtually absent in the epididymis from intact adult mice, which was filled with mature spermatozoa (Figure 5C). Many of the epididymal tH2B-immunopositive cells are round and elongating spermatids that have been prematurely released from the spermatogenic epithelium and have not undergone further elongation and nuclear condensation.

Immunostaining with an antibody against TP2 showed pronounced staining of elongated/condensing spermatids, at steps 12–14 of spermiogenesis (Alfonso and Kistler, 1993). In control mice, these spermatids are arranged in groups of cells and in a regular pattern, at stages XII and I–III of the spermatogenic cycle (Figure 5E). In *mHR6B*$^{-/-}$ mice, a relatively small number of elongated spermatids showed TP2 immunostaining, and a proportion of these cells showed abnormal morphology and were not well positioned within the spermatogenic epithelium (Figure 5F). Our findings indicate that *mHR6B*$^{-/-}$ mice synthesize TPs, but that these proteins are not uniformly located in the nucleus as observed during normal spermatogenesis.

Since the general picture is an overall impairment of spermatogenesis as a consequence of a primary defect in the elongation stage of spermiogenesis, we investigated whether apoptosis is elevated in *mHR6B*$^{-/-}$ mice. Figure 6A shows sections through seminiferous tubules of testis of 6-week-old *mHR6B* +/+ and −/− mice stained using the TUNEL assay. A 4-fold increase in the number of apoptotic cells was calculated and represented as the number of positively stained cells per 100 tubuli (Figure 6B). Moreover, the apoptotic cells were clustered and predominantly localized in the germ cell layers that contain primary spermatocytes. These data indicate an elevated level of apoptosis as a consequence of mHR6B deficiency.

Discussion

In spite of the pleiotropic functions and fundamental importance of the ubiquitin system, no mammalian mutants affected in this pathway are available that reveal the biological ramifications and impact of this process at the level of the organism. In the present report, we describe the phenotype of mice deficient in the ubiquitin-conjugating enzyme mHR6B. In both ES cells and in mice, the loss of function of *mHR6B* is compatible with viability. Although yeast *rad6* deletion mutants are viable, they display a severe phenotype. The finding that this is not the case in the *mHR6B* knockout mouse can be explained by functional redundancy of the *HR6A* and *HR6B* gene products. The hHR6A and hHR6B proteins

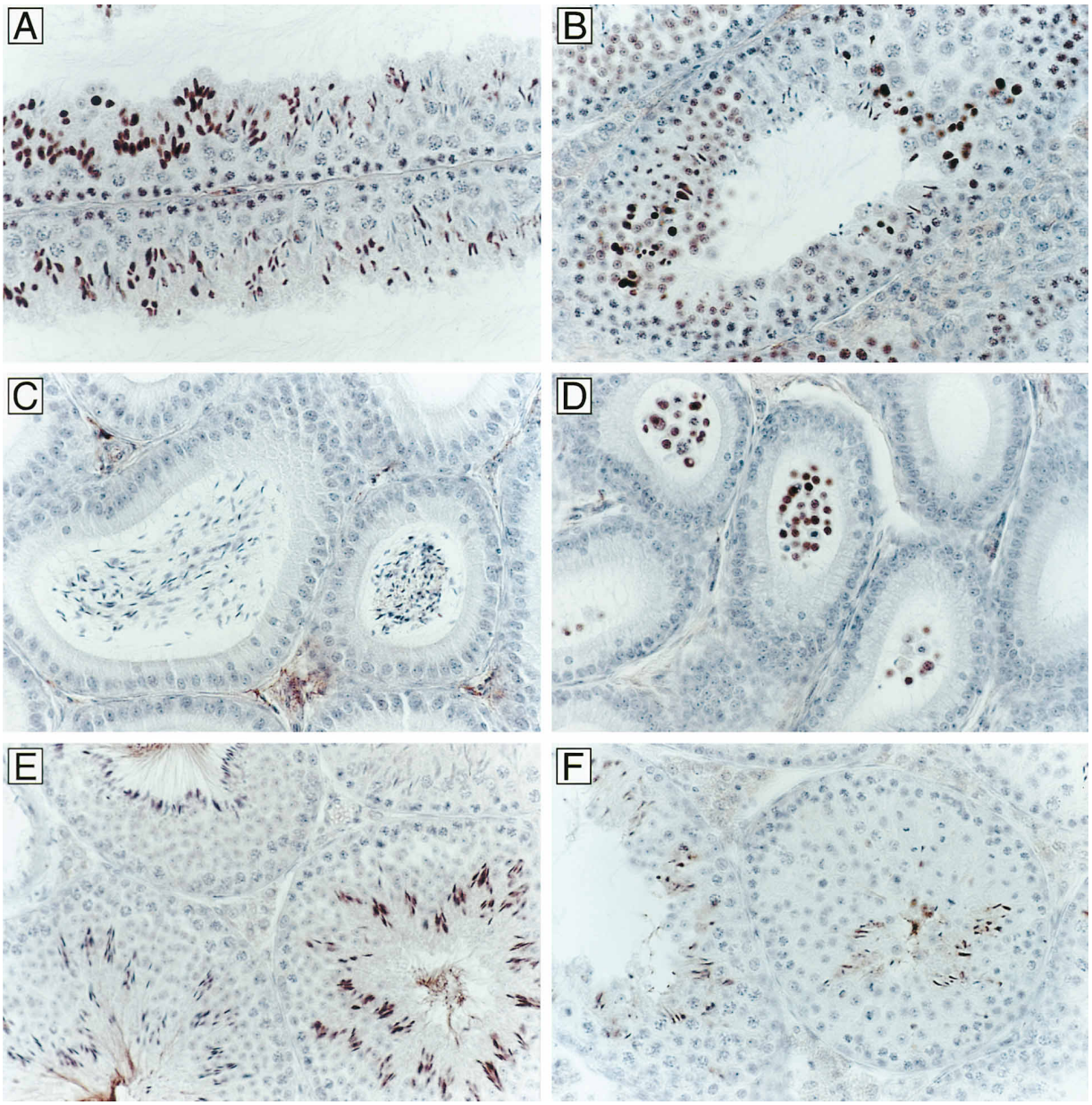

Figure 5. Immunohistochemical Localization of Testis-Specific Histone H2B and Transition Protein 2 in Testis and Epididymis of Intact and *mHR6B* Knockout Mice

The immunohistochemistry was performed as described in Experimental Procedures. The panels to the left (A, C, and E) show tissues from a 9-month-old intact mouse, and the panels to the right (B, D, and F) represent a 9-month-old *mHR6B* knockout mouse. (A) and (B): tH2B immunostaining of testis; (C) and (D): tH2B immunostaining of epididymis; (E) and (F): TP2 immunostaining of testis (×400).

are expressed to approximately the same extent in most somatic cells and tissues (Koken et al., 1996). The two gene products show 95% amino acid sequence identity and thus probably catalyze very similar reactions. Furthermore, both proteins are functional and complement the same defects of a *rad6* null allele (Koken et al., 1991b). Apparently, the ~50% of remaining activity derived from the *mHR6A* gene is sufficient to permit relatively normal development. We failed to observe any defect in DNA repair. However, this does not exclude a subtle effect of partial loss of mHR6 activity on mutagenesis and carcinogenesis, which remains to be studied. Experiments aimed at generating mHR6A-deficient mice, in order to assess the phenotype of these and full *mHR6A*/*mHR6B* double knockout mice, are in progress.

The most prominent phenotypic expression of the *mHR6B* gene knockout detected to date is impairment of spermatogenesis, resulting in greatly reduced numbers of mainly abnormal spermatids and spermatozoa. However, in the adult testis, the causative step is difficult to pinpoint, because of the considerable interindividual variation in the manifestations and the fact that early as well as late steps of spermatogenesis seem to be impaired. Detailed analysis of the first wave of spermato-

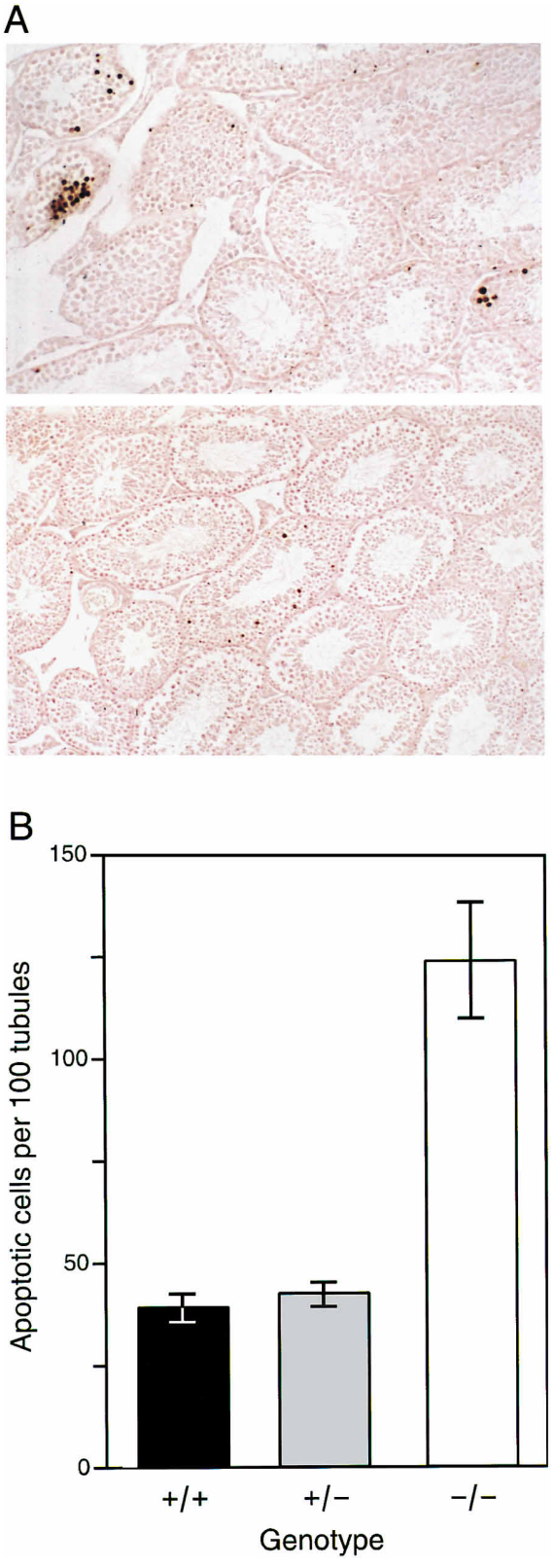

Figure 6. Analysis of Apoptosis in Seminiferous Tubule Cross Sections of Six-Week-Old Mice

(A) Nuclear DNA fragmentation visualized using the TUNEL assay. The upper panel shows a section through a testis of a homozygous mutant, and the lower panel is a testis section of a wild-type animal. A cluster of apoptotic cells is present in the upper left corner of the upper panel.

(B) Quantification of apoptosis in wild-type (+/+), heterozygous (+/−), and homozygous mutant (−/−). Slides were randomly maneuvered under a light microscope, and all apoptotic cells present in at least 100 tubule cross sections were counted and divided by the number of tubules. These data were recalculated to give the number of apoptotic cells per 100-tubule cross sections.

genesis, however, allowed identification of the primary defective stage: progression through the elongating and condensing steps of spermatid development is impaired. Probably as a secondary consequence, earlier steps of spermatogenesis also become deregulated (see below).

Previously, we found elevated levels of *mHR6A* and *mHR6B* mRNAs in spermatids during normal rat spermatogenesis (Koken et al., 1996). In fact, *HR6A* is the first X-linked gene for which postmeiotic expression, in mouse spermatids, has been documented (Hendriksen et al., 1995). In addition, immunohistochemical experiments show the presence of HR6 proteins in the nuclei of round and elongating rat spermatids. However, it is important to note that in two-dimensional immunoblot analysis of all cells tested, elongating spermatids and spermatozoa were the only cell types in which the mHR6A level appeared significantly lower relative to that of mHR6B (Koken et al., 1996). Thus, it is conceivable that in the absence of mHR6B, the relatively low levels of mHR6A are insufficient for performing the HR6 function required in these cells. Unfortunately, the low number of elongating spermatids in immature *mHR6B*$^{-/-}$ mice precludes biochemical analysis of HR6 activity in this way.

Although different hypotheses can be put forward to explain our findings, such as defects in Sertoli cells which, like germ cells, express high levels of both mHR6A and mHR6B (Koken et al., 1996), we consider the following scenario most consistent with all observations. The nuclei of early round spermatids contain a mixture of somatic histones and testis-specific histones. Following elongation of spermatids, chromatin is reorganized, and the histones are replaced by transition proteins (TPs) and then by protamines (Balhorn, 1989; Kistler, 1989; Meistrich, 1989). Two types of histone modification have been documented during spermatogenesis. In rat spermatids, occurrence of highly acetylated H4 is associated with histone displacement (Meistrich et al., 1992), and during chicken and trout spermatogenesis polyubiquitination of histone H2A has been observed (Agell et al., 1983; Nickel et al., 1987; Agell and Mezquita, 1988; Oliva and Dixon, 1991). In preliminary experiments we have detected mono- and polyubiquitinated forms of histones in nuclear extracts of mouse spermatocytes and spermatids (our unpublished data). Considering the ability of RAD6 to polyubiquitinate histones in vitro and its in vivo role in yeast sporulation, the most plausible hypothesis is that, in mammalian spermatids, the functional homologs of RAD6 polyubiquitinate histones. This allows for their degradation and replacement by transition proteins and, subsequently, by protamines. A shortage of the enzyme

at this critical stage could interfere with this process. However, it remains to be shown that the ubiquitin-conjugating enzyme activity targeting specific histones in spermatids is below a critical threshold level in spermatids from *mHR6B* knockout mice.

Spermatogenesis involves elimination and modification of many proteins. A novel ubiquitin-conjugating enzyme E2 (E2 17 kb) was recently also found to be highly expressed in testis (Wing and Jain, 1995). In addition, the Y-chromosomal gene *Sby* or *Ube1y*, encoding ubiquitin-activating enzyme E1, shows testis-specific expression in the mouse and is considered a candidate spermatogenesis gene (Kay et al., 1991; Mitchell et al., 1991). Testicular expression is dependent on the presence of germ cells (Mitchell et al., 1991) and *Ube1y* mRNA has been detected in round spermatids (Hendriksen et al., 1995). The homologous gene on the X chromosome (*Sbx* or *Ube1x*) is expressed in all male and female tissues (Mitchell et al., 1991) and also in spermatogenic cells (Hendriksen et al., 1995).

Assuming that disturbance of chromatin remodeling in spermatids of mHR6B-deficient mice is the primary cause of the infertility, how can this defect lead to formation of vacuoles in Sertoli cells and the release of immature germ cells? A clue is provided by a recent finding on the effect of ectopic expression of avian protamine (galline) in spermatids of transgenic mice. This expression induces disruption of the normal dense chromatin structure of spermatozoa, and results in infertility (Rhim et al., 1995). As for *HR6B*$^{-/-}$ mice, the spermatogenic epithelium of these transgenic males showed many vacuoles and loss of immature germ cells. Thus, disruption of chromatin conformation by ectopic protamine expression leads to very similar types of spermatogenic abnormalities as observed in *HR6B*$^{-/-}$ mice, in agreement with the idea that HR6B deficiency affects chromatin conformation. Possibly, Sertoli cells are adversely affected by degenerating late spermatids. These spermatids might release protamines, which are known to exert toxic effects on epithelial cells (Peterson and Gruenhaupt, 1992). In concordance with this, the clustered apoptosis of primary spermatocytes in testis of *mHR6B*$^{-/-}$ mice (Figure 6) points to local Sertoli cell damage.

It is not clear why most of the male *mHR6B* knockout mice show production of spermatozoa with a wide range of morphological abnormalities. Other defects in spermatogenesis affecting spermatocytes rather than spermatids, can also give rise to abnormal spermatozoa. Such a defect in spermatogenesis was observed in mice that were mutated in the DNA mismatch repair gene *PMS2* (Baker et al., 1995). This defect results in abnormal chromosomal synapsis in meiosis and male infertility, with production of a small number of spermatozoa with abnormal morphology.

In a considerable number of male infertility patients, the cause of the infertility might be related to disturbance of the histone-to-protamine replacement during spermatogenesis. Several reports describe that sperm from infertile men can show abnormal protein complements, with persistent elevated levels of histones and/or an altered protamine P1/P2 ratio (Chevaillier et al., 1987; Foresta et al., 1992; De Yebra et al., 1993). Notwithstanding the relative genetic uniformity of *HR6B*$^{-/-}$ mice, a marked variation of testis histology and sperm morphology was observed. The pronounced variability in features is reminiscent of the testicular manifestations associated with infertility in man. The fact that an HR6B defect in mice can be transmitted not only by heterozygous carriers but even by homozygous knockout females enhances the possibility that the identical human enzyme may be implicated in male infertility conditions. Probably as many as one in three of all cases of human male infertility are of unknown testicular origin. These cases cannot be explained by chromosome abnormalities, endocrine dysfunction, etc. (Wong et al., 1973). In unexplained male infertility, there is often the production of a low number of spermatozoa (oligozoospermia) and/or abnormal sperm morphology (teratozoospermia) (Aitken et al., 1995). Several hallmarks of this variable condition are shared with *HR6B*$^{-/-}$ mice. A potential involvement of a defect in the ubiquitin pathway in cases of human male infertility is presently under investigation.

A final implication from the findings reported here is the parallel emerging between spermatogenesis in mammals and sporulation in yeast (Game and Mortimer, 1974; Montelone et al., 1981). The latter process also appeared to be accompanied by gross changes in chromatin conformation in which RAD6 may play a similar role as HR6B in higher organisms. Interestingly, the yeast UBC1 enzyme is found to be required for recovery of growth after germination of ascospores (Jentsch, 1992). This enzyme may thus accomplish the reverse of the reaction catalyzed by RAD6, namely the decondensation of chromatin.

Experimental Procedures

Isolation and Sequence of Murine *mHR6B* cDNA Clones

A 784 bp HindIII-BamHI cDNA fragment containing the complete open reading frame (ORF) of the human *HhR6B* gene, including 5′ and 3′ flanking sequences (176 and 149 nucleotides, respectively) (Koken et al., 1996), was used to screen a 129/Ola mouse testis library (λZAP) for *hHR6B* homologous mouse cDNAs. Seven positive plaques were isolated of which 2 contained the complete ORF. The nucleotide sequence of the ORF of *mHR6B* and (part of) the 3′ untranslated region were determined using T7-polymerase (Pharmacia Biotech, Uppsala, Sweden) and deposited in the GenBank/EMBL nucleotide sequence database under accession number X96859.

Construction of the Mouse *mHR6B*-Targeting Vector and Transfection

An EMBL-3 λ phage genomic library constructed from the CCE ES cell line derived from mouse strain 129/Sv (a gift of Dr. G. Grosveld) was screened with the 784 bp human *HR6B* cDNA fragment. Positive genomic clones were rescreened with a [γ-^{32}P]ATP primer, complementary to nucleotides 28–69 of the mouse *HR6B* coding region. A genomic clone was isolated, designated G28, encompassing the exons encoding the 5′ end of the *mHR6B* coding region. This genomic clone was digested with SalI and subcloned in pTZ19R (Pharmacia Biotech). The two SalI subclones flanking the SalI-site at the 5′ end of the ORF were cloned into the vector pGEM-7Zf(+) (Promega Corp., Madison, WI). In this way, a unique KpnI-site was created at this position. A cassette with the neomycin resistance gene driven by the TK-promoter (Thomas and Capecchi, 1987) was inserted at this KpnI site, resulting in a targeting vector with 3.2 and 3.5 kb of homologous sequences flanking the mutation at the 3′ and 5′ position, respectively. This *neo* cassette was inserted in the antisense orientation with respect to the transcriptional orientation of the *mHR6B* gene. The resulting plasmid was linearized with NsiI, reducing the homologous region 3′ of the *neo* cassette to 2.8 kb, and

electroporated into 129/Ola-derived E14 ES cells (a gift of Dr. A. Berns, NKI, Amsterdam, The Netherlands) as described earlier (Zhou et al., 1995). G418 (Geneticin; GIBCO–BRL, Gaithersburg, MD) was added 24 hr after electroporation (final concentration: 200 μg/ml), and the cells were maintained under selection for 6–8 days. Genomic DNA from individual, neomycin-resistant clones was digested with EcoRI or SphI and analyzed by Southern blotting using a 0.7 kb EcoRI–EcoRV probe positioned immediately 3′ of the targeting construct. Targeted clones, with the correct hybridizing EcoRI fragments, were subsequently screened with a fragment of the *neo*-resistance gene as a probe to confirm proper homologous recombination.

To obtain double targeted ES cells, a second targeting construct was made in a similar way with a cassette containing a hygromycin resistance gene under the control of the PGK-promoter (Riele te et al., 1990) instead of the *neo* cassette.

Generation of mHR6B-Deficient Mice

Cells of G418-resistant, homologous recombinant clones were karyotyped and ES cells from two independent clones with 40 normal chromosomes were used for injection into 3.5-day-old blastocysts isolated from pregnant C57BL/6 females as described previously (Zhou et al., 1995). Male chimaeric mice were mated with FVB/J females to obtain heterozygote animals. Germline transmission was observed in the coat color of the F1 offspring. Genomic DNA was isolated from tail biopsies, digested with EcoRI, resolved in 1% agarose, blotted, and probed with the 0.7 kb EcoRI–EcoRV diagnostic probe to assess the genotype (Figure 1A). Heterozygous siblings were mated to generate *mHR6B*$^{-/-}$ animals.

Antibody Production and Immunoblotting

A peptide of 15 amino acids, resembling the C-terminal end of the mHR6B/hHR6B protein including an additional cysteine, KRVSAIVE QSWNDSC, was synthesized on an automated peptide synthesizer (Novabiochem AG, Laüfelfingen, Switzerland) as described earlier (Koken et al., 1996). One milligram peptide was dissolved in phosphate-buffered solution (PBS) and coupled to activated carrier protein (keyhole lampet hemocyanin) according to the manufacturer's guidelines (Pierce, Rockford, IL). A rabbit was primed by intracutaneous application of the antigen mixed with Freund's complete adjuvans. The first boost of the antigen was applied after 5 weeks and the second boost after 10 weeks. For boosting the antigen was mixed with Freund's incomplete adjuvans. Blood was collected 14 days after the second boost. Preparation of crude tissue extracts, separation of sample contents, electroblotting, and antigen detection were carried out as described by Koken et al. (1996). The primary antibody, raised against the C-terminal petide, was used in a 1:250 dilution. The blots were developed using horseradish peroxidase (Biosource International, Camarillo, CA) as the secondary antibody and visualized using ECL (Amersham International plc, Little Chalfont, England).

Cell Survival after Irradiation

UV sensitivity was determined assaying the incorporation of [^{3}H]thymidine by proliferating fibroblasts at various doses of UV. In short, cells were pulse-labeled for 1 hr, incubated in unlabeled medium for 1 hr, lysed, and incorporation was quantified using a scintillation counter. Cell survival is expressed as the ratio of ^{3}H incorporation in irradiated and nonirradiated primary mouse embryonic fibroblasts (A. M. Sijbers et al., submitted).

Ionizing radiation sensitivity was determined by comparing the colony-forming ability of targeted ES cells after ^{60}Co-irradiation essentially as described by (Taalman et al., 1983). After irradiation, cells were seeded on BRL-conditioned ES medium in 60 mm petridishes. Cells were grown for 6–10 days, fixed, and stained. The number of colonies were counted and compared with nontargeted ES cells treated in the same way.

Hormone and Tissue Weight Determination

Blood was collected by orbital sinus puncture under ether anaesthesia. Then, the animals were killed by cervical dislocation, and the testes, epididymides, and seminal vesicles were dissected out. Of each animal, one testis and its attached epididymis were fixed using Bouin's solution, and the other testis and epididymis were weighed. The latter epididymis was homogenized in phosphate-buffered saline, to count the number of spermatozoa using a Neubauer haemocytometer. Cells with a head and a tail were regarded as sperm cells, irrespective of morphological abnormalities.

The concentration of FSH in the circulation was estimated by radioimmunoassay in 2 volumes of serum (Dullaart et al., 1975). The concentration of FSH is expressed in terms of the standard NIDDK RP-2. The interassay coefficient of variation was 10%.

Histology

Testes were isolated and punctured for good penetration of the fixative. Testes and epididymides were fixed for 48 hr in Bouin's fixative at room temperature, the fixative was extracted with 70% ethanol for 2–3 days, and the tissues were embedded in paraffin. Mounted sections (4–6 μm) were deparaffinized, rehydrated, and stained with the periodic acid/Schiff sulfite leucofuchsin (PAS) reaction or used in immunohistochemistry.

Immunohistochemistry

Immunohistochemical localization of TP2 was performed using rabbit anti-rat polyclonal antibody (Alfonso and Kistler, 1993) (kindly provided by Dr. Kistler). Immunolocalization tH2B was performed using a mouse monoclonal IgG raised against tyrosine hydroxylase (TH; Boehringer Mannheim GmbH, Mannheim, Germany), which is known to also immunoreact with rat tH2B in tissue sections because of sequence homology at the N-termini of TH and tH2B (Unni et al., 1995).

Testis and epididymis sections were mounted on slides coated with 3-aminopropyltrietoxysilane (Sigma Co., St. Louis, MO), and kept at 60°C overnight. The tissues were dewaxed in xylene, and endogenous peroxidase was blocked with a 20 min incubation in 3% H_2O_2 in methanol. An antigen retrieval step was performed, for tissues prepared for anti-TP2 staining, by heating the sections in 0.01 M sodium citrate buffer (pH 6.0) in a microwave oven at 700 W (4 × 5 min). This was not necessary for sections prepared for anti-TH immunostaining. Nonspecific antibody binding was blocked with normal goat serum (Dako, Glostrup, Denmark), diluted 1:10 in 5% (w/v) bovine serum albumin (BSA) in PBS (pH 7.4). The tissues were then placed in a Sequenza immunostainer (Shandon Scientific Ltd., Runcorn, England) and incubated at 4°C overnight with the primary antibody, diluted 1:10,000 for anti-TP2 and 1:100 for anti-TH in 5% BSA (w/v) in PBS. Immunostaining was performed using biotinylated goat anti-rabbit or goat anti-mouse immunoglobulin where appropriate (Dako) for 30 min, streptavidin-peroxidase (Dako) for 30 min, and metal-enhanced diaminobenzidine (Pierce) for 7 min. The sections were counterstained for 15 s with Mayer's hematoxylin and viewed with a Zeiss Axioskop 20 light microscope at magnifications 100× and 400×. Control sections were incubated with 5% BSA (w/v) in PBS without the primary antibody and subsequently processed as described above.

Nuclear DNA Fragmentation Labeling (TUNEL)

Tissues were fixed for 16 hr at 4°C in PBS containing 3.6% formaldehyde and embedded in paraffin. Sections (4–6 μm) were mounted on AAS-coated glass slides, dewaxed, and pretreated with proteinase-K (Sigma) and peroxidase as described elsewhere (Gavrieli et al., 1992). Slides were subsequently washed in TdT-buffer for 5 min (Gorczyca et al., 1993) and incubated for at least 30 min in TdT-buffer containing 0.01 mM Biotin-16-dUTP (Boehringer Mannheim) and 0.4 U/μl TdT-enzyme (Promega). The enzymatic reaction was stopped by incubation in TB-buffer and the sections were washed (Gavrieli et al., 1992). Slides were then incubated with streptABComplex/horseradish peroxidase conjugate (Dako) for 30 min and washed in PBS. dUTP-biotin-labeled cells were visualized with Diaminobenzidine.4HCl (Sigma). Cells were counterstained with 0.2% (w/v) nuclear fast red/5% (w/v) $Al_2(SO_4)_3$ for 10 s and rinsed in tap water for 10 min.

Acknowledgments

The authors are indebted to Dr. G. Weeda and I. Donker for advice and instructions with the mouse embryo technology. Antibodies

targeting TP2 were kindly provided by Dr. S. Kistler. Prepublished information concerning immunohistochemistry of tH2B was made available to us by Dr. M. Meistrich. We would like to thank Drs. S. Kistler and M. Meistrich for their valuable advice and discussions, M. Kuit for photographic work, and Dr. M. McKay for critically reading the manuscript. The work was supported by the Dutch Cancer Society (IKR 92–118 and 88–02), and the Division of Medical Sciences of the Dutch Scientific Organization (NWO, projects 900–501–093 and 903–44–138).

Received April 17, 1996; revised July 1, 1996.

References

Agell, N., and Mezquita, C. (1988). Cellular content of ubiquitin and formation of ubiquitin conjugates during chicken spermatogenesis. Biochem. J. *250*, 883–889.

Agell, N., Chiva, M., and Mezquita, C. (1983). Changes in nuclear content of protein conjugate histone H2A-ubiquitin during rooster spermatogenesis. FEBS Lett. *155*, 209–212.

Aitken, R.J., Baker, H.W.G., and Irvine, D.S. (1995). On the nature of semen quality and infertility. Hum. Reprod. *10*, 248–249.

Alfonso, P.J., and Kistler, W.S. (1993). Immunohistochemical localization of spermatid nuclear transition protein 2 in the testes of rats and mice. Biol. Reprod. *48*, 522–529.

Baker, S.M., Bonner, C.E., Zhang, L., Plug, A.W., Robatzek, M., Warren, G., Elliott, E.A., Yu, J., Ashley, T., Arnheim, N., et al. (1995). Male mice defective in the DNA mismatch repair gene *PMS2* exhibit abnormal chromosome synapsis in meiosis. Cell *82*, 309–319.

Balhorn, R. (1989). Mammalian protamines: structure and molecular interactions. In Molecular Biology of Chromosome Function, K.W. Adolph, ed. (New York: Springer), pp. 366–395.

Brock, W.A., Trostle, P.K., and Meistrich, M.L. (1980). Meiotic synthesis of testis histones in the rat. Proc. Natl. Acad. Sci. USA *77*, 371–375.

Chau, V., Tobias, J.W., Bachmair, A., Marriott, D., Ecker, D.J., Gonda, D.K., and Varshavsky, A. (1989). A multiubiquitin chain is confined to specific lysine in a targeted short-lived protein. Science *243*, 1576–1583.

Chevaillier, P., Mauro, N., Feneux, D., Jouannet, P., and David, G. (1987). Anomalous protein complement of sperm nuclei in some infertile men. Lancet *2*, 806–807.

Ciechanover, A. (1994). The ubiquitin-proteasome proteolytic pathway. Cell *79*, 13–21.

Ciechanover, A., DiGiuseppe, J.A., Bercovich, B., Orlan, A., Richter, J.D., Schwartz, A.L., and Brodeur, G.M. (1991). Degradation of nuclear oncoproteins by the ubiquitin proteolysis system in vitro. Proc. Natl. Acad. Sci. USA *88*, 139–143.

De Yebra, L., Ballescà, J.L., Vanrell, J.A., Bassas, L., and Oliva, R. (1993). Complete selective absence of protamine P2 in humans. J. Biol. Chem. *268*, 10553–10557.

Dohmen, R.J., Madura, K., Bartel, B., and Varshavsky, A. (1991). The N-end rule is mediated by the UBC2 (RAD6) ubiquitin-conjugating enzyme. Proc. Natl. Acad. Sci. USA *88*, 7351–7355.

Dullaart, J., Kent, J., and Ryle, M. (1975). Serum gonadotrophin concentrations in infantile female mice. J. Reprod. Fertil. *43*, 189–192.

Foresta, C., Zorzi, M., Rossata, M., and Varotto, A. (1992). Sperm nuclear instability and staining with aniline blue: abnormal persistance of histones in spermatozoa in infertile men. Int. J. Androl. *15*, 330–337.

Game, J.C., and Mortimer, R.K. (1974). A genetic study of X-ray sensitive mutants in yeast. Mutation Res. *24*, 281–292.

Gavrieli, Y., Sherman, Y., and Ben-Sasson, S.A. (1992). Identification of programmed cell death in situ via specific labeling of nuclear DNA fragmentation. J. Cell Biol. *119*, 493–501.

Glotzer, M., Murray, A.W, and Kirschner, M.W. (1991). Cyclin is degraded by the ubiquitin pathway. Nature *249*, 132–138.

Goldknopf, I.L., and Busch, H. (1980). N-bromosuccinimide fragmentation of protein A24 (uH2A): a indication that ubiquitin is the precursor of conjugation *in vivo*. Biochem. Biophys. Res. Commun. *96*, 1724–1731.

Gorczyca, W., Gong, J., and Darzynkiewicz, Z. (1993). Detection of DNA strand breaks in individual apoptotic cells by the in situ terminal deoxynucleotidyl transferase and nick translation assays. Cancer Res. *53*, 1945–1951.

Hendriksen, P.J.M., Hoogerbrugge, J.W., Themmen, A.P.N., Koken, M.H.M., Hoeijmakers, J.H.J., Oostra, B.A., Van der Lende, T., and Grootegoed, J.A. (1995). Postmeiotic transcription of X and Y chromosomal genes during spermatogenesis in the mouse. Dev. Biol. *170*, 730–733.

Hochstrasser, M. (1995). Ubiquitin, proteasomes, and the regulation of intracellular protein degradation. Curr. Opin. Cell Biol. *7*, 215–223.

Jentsch, S. (1992). Ubiquitin-dependent protein degradation: a cellular perspective. Trends Cell Biol. *2*, 98–103.

Jentsch, S., McGrath, J.P., and Varshavsky, A. (1987). The yeast DNA repair gene RAD6 encodes a ubiquitin-conjugating enzyme. Nature *329*, 131–134.

Kay, G.F., Ashworth, A., Penny, G.D., Dunlop, M., Swift, S., Brockdorff, N., and Rastan, S. (1991). A candidate spermatogenesis gene on the mouse Y chromosome is homologous to ubiquitin-activating enzyme E1. Nature *354*, 486–489.

Kistler, W.S. (1989). Structure of testis-specific histones, spermatid transition proteins, and their genes in mammals. In Histones and Other Basic Nuclear Proteins., L.S. Hnilica, G.S. Stein, and J.L. Stein, eds. (Boca Raton, Florida: CRC Press), pp. 331–346.

Koken, M., Reynolds, P., Bootsma, D., Hoeijmakers, J., Prakash, S., and Prakash, L. (1991a). *Dhr6*, a *Drosophila* homolog of the yeast DNA-repair gene RAD6. Proc. Natl. Acad. Sci. USA *88*, 3832–3836.

Koken, M.H.M., Reynolds, P., Jaspers-Dekker, I., Prakash, L., Prakash, S., Bootsma, D., and Hoeijmakers, J.H.J. (1991b). Structural and functional conservation of two human homologs of the yeast DNA repair gene RAD6. Proc. Natl. Acad. Sci. USA *88*, 8865–8869.

Koken, M.H.M., Hoogerbrugge, J.W., Jaspers-Dekker, I., de Wit, J., Willemsen, R., Roest, H.P., Grootegoed, J.A., and Hoeijmakers, J.H.J. (1996). Expression of the ubiquitin-conjugating DNA repair enzymes HHR6A and B suggests a role in spermatogenesis and chromatin modification. Dev. Biol. *173*, 119–132.

Kornitzer, D., Raboy, B., Kulka, R.G., and Fink, G.R. (1994). Regulated degradation of the transcription factor Gcn4. EMBO J. *13*, 6021–6030.

Lawrence, C. (1994). The *RAD6* repair pathway in *Saccharomyces cerevisiae*: what does it do, and how does it do it? BioAssays *16*, 253–258.

Madura, K., Dohmen, R.J., and Varshavsky, A. (1993). N-recognin/Ubc2 interactions in the N-end rule pathway. J. Biol. Chem. *268*, 12046–12054.

Meistrich, M.L. (1989). Histone and basic nuclear protein transitions in mammalian spermatogenesis. In Histones and Other Basic Nuclear Proteins, L.S. Hnilica, G.S. Stein, and J.L. Stein, eds. (Boca Raton, Florida: CRC Press), pp. 165–182.

Meistrich, M.L., Bucci, L.R., Trostle-Weige, P.K., and Brock, W.A. (1985). Histone variants in rat spermatogonia and primary spermatocytes. Dev. Biol. *112*, 230–240.

Meistrich, M.L., Trostle-Weige, P.K., Lin, R., Bhatnagar, Y.M., and Allis, C.D. (1992). Highly acetylated H4 is associated with histone displacement in rat spermatids. Mol. Reprod. Dev. *31*, 170–181.

Mitchell, M.J., Woods, D.R., Tucker, P.K., Opp, J.S., and Bishop, C.E. (1991). Homology of a candidate spermatogenesis gene from the mouse Y chromosome to the ubiquitin-activating enzyme E1. Nature *354*, 483–486.

Montelone, B.A., Prakash, S., and Prakash, L. (1981). Recombination and mutagenesis in *rad6* mutants of *Saccharomyces cerevisiae*: evidence for multiple functions of the *RAD6* gene. Mol. Gen. Genet. *184*, 410–415.

Nickel, B.E., Roth, S.Y., Cook, R.G., Allis, C.D., and Davie, J.R. (1987). Changes in the histone H2A variant H2A. Z and polyubiquitinated

histone species in developing trout testis. Biochemistry *26*, 4417–4421.

Oliva, R., and Dixon, G.H. (1991). Vertebrate protamine genes and the histone-to-protamine replacement reaction. Progr. Nucleic Acid Res. Mol. Biol. *40*, 25–94.

Peterson, M.W., and Gruenhaupt, D. (1992). Protamine interaction with the epithelial cell surface. J. Appl. Physiol. *72*, 236–241.

Reynolds, P., Koken, M.H.M., Hoeijmakers, J.H.J., Prakash, S., and Prakash, L. (1990). The *rhp6*+ gene of *Schizosaccharomyces pombe*: a structural and functional homolog of the *RAD6* gene from the distantly related yeast *Saccharomyces cerevisiae*. EMBO J. *9*, 1423–1430.

Rhim, J.A., Connor, W., Dixon, G.H., Harendza, C.J., Evenson, D.P., Palmiter, R.D., and Brinster, R.L. (1995). Expression of an avian protamine in transgenic mice disrupts chromatin structure in spermatozoa. Biol. Reprod. *52*, 20–32.

Riele te, H., Robonus Maandag, E., Clarke, A., Hooper, M., and Berns, A. (1990). Consecutive inactivation of both alleles of the *pim-1* proto-oncogene by homologous recombination in embryonic stem cells. Nature *348*, 649–651.

Roller, M.L., Lossie, A.C., Koken, M.H.M., Smit, E.M.E., Hagemeijer, A., and Camper, S.A. (1995). Localization of sequences related to the human *RAD6* DNA repair gene on mouse chromosomes 11 and 13. Mamm. Genome *6*, 305–306.

Russell, L.D., Ettlin, R.A., Sinha Hikim, A.P., and Clegg, E.D. (1990). Histological and Histopathological Evaluation of the Testis. (Clearwater, Florida: Cache River Press).

Scheffner, M., Nuber, U., and Huibregtse, J.M. (1995). Protein ubiquitination involving an E1-E2-E3 enzyme ubiquitin thioester cascade. Nature *373*, 81–83.

Schneider, R., Eckerskorn, C., Lottspeich, F., and Schweiger, M. (1990). The human ubiquitin carrier protein E2(M_r = 17 000) is homologous to the yeast DNA repair gene RAD6. EMBO J. *9*, 1431–1435.

Seufert, W., Futcher, B., and Jentsch, S. (1995). Role of a ubiquitin-conjugating enzyme in degradation of S- and M-phase cyclins. Nature *373*, 78–81.

Taalman, R.D.F.M., Jaspers, N.G.J., Scheres, J.M.J.C., de Wit, J., and Hustinx, T.J.W. (1983). Hypersensitivity to ionizing radiation, in vitro, in a new chromosomal breakage disorder, the Nijmegen Breakage Syndrome. Mutation Res. *112*, 23–32.

Thomas, K.R., and Capecchi, M.R. (1987). Site-directed mutagenesis by gene targeting in mouse embryo-derived stem cells. Cell *51*, 503–512.

Thorne, A.W., Sautiere, P., Briand, G., and Crane-Robinson, C. (1987). The structure of ubiquitinated histone H2B. EMBO J. *6*, 1005–1010.

Unni, E., Mayerhofer, A., Zhang, Y., Bhatnagar, Y.M., Russell, L.D., and Meistrich, M.L. (1995). Increased accessibility of the N-terminus of testis-specific histone TH2B to antibodies in elongating spermatids. Mol. Reprod. Dev. *42*, 210–219.

Wing, S.S., and Jain, P. (1995). Molecular cloning, expression and characterization of a ubiquitin enzyme (E217kD) highly expressed in rat testis. Biochem. J. *305*, 125–132.

Wong, T.-W., Straus, F.H., and Warner, N.E. (1973). Testicular biopsy in the study of male infertility. Arch. Pathol. *95*, 151–159.

Zhou, X.Y., Morreau, H., Rottier, R., Davis, D., Bonten, E., Gillemans, N., Wenger, D., Grosveld, F.G., Doherty, P., Suzuki, K., et al. (1995). Mouse model for the lysozomal disorder galactosialidosis and correction of the phenotype with overexpressing erythroid precursor cells. Genes Dev. *9*, 2623–2634.